J. Appl. Comput. Mech., 11(1) (2025) 82-97
DOI: 10.22055/jacm.2024.46643.4563

ISSN: 2383-4536
jacm.scu.ac.ir

Shahid Chamran University of Ahvaz

Journal of Applied and Computational Mechanics

Research Paper

Free Convective Flow of Conducting Hybrid Nanofluid between a Rotating Cone and Circular Disc: Response of Nusselt Number Utilizing Various Factors

Rupa Baithalu[1], Subhajit Panda[2], S.R. Mishra[1]

[1] Department of Mathematics, Siksha 'O' Anusandhan University, Bhubaneswar, Odisha 751030, India,
Email: rupadhananjaygarnaik@gmail.com (R.B.); satyaranjan_mshr@yahoo.co.in (S.R.M.)

[2] Center for Data Science, Siksha 'O' Anusandhan University, Bhubaneswar, Odisha 751030, India, Email: spanda.math@gmail.com

Received April 17 2024; Revised May 16 2024; Accepted for publication June 03 2024.
Corresponding author: S.R. Mishra (satyaranjan_mshr@yahoo.co.in)

Abstract. The present investigation focuses on examining the thermophysical characteristics of flow in a gap between rotating cone and circular discs utilizing hybrid nanofluids, owing to its varied applications. The enhanced thermal conductivity of nanofluids proves particularly valuable in cooling systems, diminishing energy consumption, preventing overheating, and enhancing the overall performance of electronic devices, among other benefits. The convectional flow of conductive fluid under the influence of magnetic field and thermal radiation significantly influences the flow dynamics. Moreover, the consideration of dissipative heat, including the combined effects of viscous and Joule dissipation, amplifies the flow properties. The complex nonlinear system of equations, initially presented in dimensional form, undergo transformation into a nonlinear ordinary system in non-dimensional form through the introduction of appropriate similarity rules. Various profiles are then generated using bvp4c built-in function supported in MATLAB and depicted graphically. To optimize the responsiveness of Nusselt number with respect to various factors, a robust statistical approach known as response surface methodology is employed. Statistical validation is carried out using analysis of variance through hypothetical testing.

Keywords: Hybrid nanofluid; Rotating cone and circular disc; Joule dissipation; Response surface methodology; Analysis of variance.

1. Introduction

Hybrid nanofluid, a novel class of fluids, combines nanoparticles with conventional base fluids. This combination of elements results in substantially improved thermal conductivity in contrast to conventional heat transportation liquids. The unique combination of nanoparticles and base liquid properties leads to improved heat transfer efficiency. Hybrid nanofluids hold great promise for various engineering applications requiring efficient thermal management. These nanofluids are increasingly being employed in cooling systems for electronic devices, automobiles, and industrial machinery. Hybrid nanofluids have shown potential in biomedical applications such as hyperthermia cancer treatment and cryopreservation. Raza et al. [1] investigated the dynamics of simultaneous thermal and mass transmission in nanolayers driven by morphology, magnetohydrodynamics (MHD), and motile microorganisms. Additionally, their study explored the notable influence of viscous dissipation resulting from joule heating effects on the flow features of ternary hybrid nanofluids, encompassing both model and nanolayer thermal conductivity. Panda et al. [2] presented the Williamson fluid flowing through two inclined parallel sheets. Additionally, the significant association of heat radiation and heating through osmosis are discussed. Moreover, the "*Homotopy perturbation method (HPM)*" is implemented analytically to the finalized renovated equations. Mishra et al. [3] examined how particle shape influences the radiative motion of a Casson hybridized nano liquid towards an elastic or diminishing convective sheet. Furthermore, the hybrid nanofluid discussed in this investigation consists of water and carbon nanotubes (CNTs) with varying particle shapes. A Casson-type model is utilized to determine the nanofluid's rheological property while accounting for the fluid's non-Newtonian dynamics. Rana et al. [4] investigated thermal buoyancy-driven dynamics of Ag-MgO hybrid nanoliquids using "*Finite Element Method*" analysis. Finally, the response surface method is employed to optimize both the drag force and the heat transport rate. Ramzan et al. [5] examined the flow behavior of ternary hybrid nanofluid across cone and wedge. Additionally, they employed a homotopic analysis approach to facilitate the semi-analytical derivation of the established model. Ahmed and colleagues [6-7] explored solutions for the square lid-driven cavity under an inclined magnetic field, alongside investigating homogeneous and heterogeneous reactions within the magnetohydrodynamic boundary layer of a stalled flow of an Al_2O_3-Cu-water equipped hybrid nanoliquid past an elastic decreasing sheet. The mathematical formulation reduced the problem using the "*Coiflet wavelet homotopy approach*". The findings indicate that their proposed approach exhibits superior characteristics and robust nonlinear processing capabilities compared to both the "*Coiflet wavelet analysis method*" and the traditional homotopy analysis method, rendering it more suitable for addressing intricate nonlinear problems. In the study conducted by Baithalu et al. [8], an investigation was carried out on the flow of a polar hybridized nanoliquid over an elastic interface. The study emphasized the significance of both shear rate as well as couple stresses in influencing the flow behavior. Furthermore, the association of Ag and MoS4 nanoparticles within a water-based fluid on the collective flow features. Their work employed the "*Response Surface Methodology*" (RSM) along with "*Analysis of Variance*" (ANOVA) to optimize key factors, contributing to a comprehensive analysis of the fluid flow dynamics. Ahmed et al. [9] explored the dynamics of a hybridised nanoliquid flowing through a microchannel under the influence of a time-dependent periodic pressure gradient. Furthermore, their work incorporates the occurrence of an electric double layer, magnetic field, and thermal radiation effects. Moreover, electrostatic potential is modelled using the Boltzmann-Poisson equation, while the conservation of momentum and thermal energy is described by employing the reduced Navier-Stokes equations, assuming small pressure amplitudes. Acharya [10] examined the flow of a hybrid nanofluid comprising MWCNT-Fe3O4 particles dispersed in water through a micro-wavy channel. Additionally, the governing equations were solved utilizing the "*Galerkin-finite-element scheme*". Moreover, numerical analysis indicates that altering the amplitude-based wavy texture, whether increasing or decreasing it, enhances flow dynamics and promotes heat transfer more effectively compared to surfaces with a uniform amplitude-based wavy texture. Acharya [11] investigated the effects of the solid-liquid interfacial layer as well as nanocomposite diameter on transient ferrous-water nanoliquid flowing across a spinning disc. The governing equations are solved using the "*spectral quasilinearization technique*" and the residual error profile. Bartwal et al. [12] explored a modified Fourier's law within a fuzzy environment to investigate the movement of tangent hyperbolic fluid towards a non-flat widening sheet. Utilizing the LWCM approach, the thermal and mass transmission phenomena in different flow scenarios have been carried out. The contribution of several physical factors that are vital in various engineering as well as industrial applications is deliberated briefly. Further, the association of melting heat transmission and magnetohydrodynamics (MHD) on stagnation point flowing over a porous rotating disk, focusing on tangent hyperbolic fluid have been proposed by Bartwal et al. [13-14]. The transformed flow phenomena are handled numerically and the analysis of the physical parameters are deliberated clearly and the result reveals the structural improvement of these factors. Mishra et al. [15] explored a transverse magnetised field which is in the motion of a non-Newtonian polar fluid influence the transmission phenomena in a double stratified restriction. Francis et al. [16] deliberated the behaviour of non-Newtonian nanofluids on a cone's surface. Additionally, the ODEs are numerically solved with MATLAB's bvp4c solver. Ratha et al. [17] focused on the behavior of electrically conducting nanofluids containing oxide nanoparticles within a fluid environment comprising submerged water and ethylene glycol as base fluids. This study delves into the flow dynamics surrounding a radially stretching sheet, which is positioned within a permeable medium. The governing equations are reconfigured through suitable similarity transformations, achieved through both the "*Differential Transform Method*" and the "*Pade-Approximant technique*". Li et al. [18] investigated the impact of a transverse magnetism on the free convection of an unsteady, electrically conducting nanofluid towards a vertical sheet embedded within a porous medium. Thumma et al. [19] employed numerical methods to investigate the impact of nonlinearity in temperature-dependent density and the impact of a non-uniform heat source/sink on the three-dimensional flow of a Maxwell nanofluid towards an elastic surface. To solve these dimensionless ODEs, a "*fourth-order Runge-Kutta method*" combined with the "*shooting technique*" is employed. Mahmud et al. [20] investigated the movement of oxytactic microorganisms subjected to the Lorentz force as they traverse a porous Riga surface. The study employs a nano fluid rheological model with couple stress as the working fluid. Numerical solutions to the main equations, expressed in non-dimensional parameters, are obtained using the shooting method.

1.1. Focus point of the study

The proposed literatures presented above lead to following properties showing focus point of the study:

- Investigate the thermophysical properties of flow within a rotating cone and circular disc utilizing hybrid nanofluids.
- Analyze the free convective flow of conducting hybrid nanofluid under the influence of magnetic fields and thermal radiation.
- Explore the effects of dissipative heat, including viscous and Joule dissipation on flow properties.
- A robust statistical approach is implemented for the optimized heat transmission rate utilizing several factors.
- Evaluate the impact of hybrid nanofluids on cooling systems to reduce energy consumption and prevent overheating of electronic gadgets.

1.2. Novelty of the proposed investigation

The contribution of the current study can be summarized as follows:

- The flow characteristics of hybrid nanofluid are proposed within the gap among the rotating cone and circular disc.
- The combined impact of magnetic field and thermal radiation on free convective flow shows complexity in nature which is reflected in flow phenomena.
- Consideration of dissipative heat effects, including viscous and Joule dissipation are useful in enhancing the effectiveness of the study.
- Development and application of a statistical approach such as response surface methodology, for optimizing the response to various factors is vital.
- The enhanced thermal conductivity of nanofluids has specific benefits of in various applications, including cooling systems and electronic devices.

2. Mathematical Formulation

The study focuses on convective heat transfer between two conical gaps a stationary or spinning cone and a disc, both carrying an incompressible viscous fluid, as illustrated in Fig. 1. Shevchuk [21] demonstrated the physical phenomenon using a radially varying wall temperature $T_w = T_\infty + cr^n$ on the disc surface, where the uniform temperature along the cone wall is T_∞ and c and n are constants. The system presented in [21] articulates the complete axisymmetric fluid flow equations, incorporating the standard continuity and Navier-Stokes equations tailored for the flow arrangement described in cylindrical coordinates (r,ϕ,z), as depicted in Fig. 1.

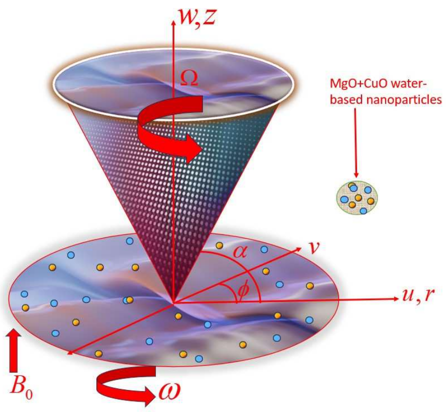

Fig. 1. Schematic representation of the current study.

Based on the aforementioned assumptions, the standard equations are:

$$ru_r + u + rw_z = 0, \tag{1}$$

$$\rho_{nf} r\left(ruu_r - v^2 + rwu_z\right) = -r^2 P_r + \mu_{nf}\left[r^2 u_{rr} + ru_r - u + r^2 u_{zz}\right] - \sigma_{hnf} B_0^2 r^2 u + r^2 g(\rho\beta_T)_{hnf}(T - T_\infty), \tag{2}$$

$$\rho_{hnf} r\left(ruv_r + uv + rwv_z\right) = \mu_{hnf}\left[r^2 v_{rr} + ru_r - v + r^2 v_{zz}\right] - \sigma_{hnf} B_0^2 r^2 v, \tag{3}$$

$$\rho_{hnf} r\left(uw_r + ww_z\right) = -rP_z + \mu_{hnf}\left[rw_{rr} + w_r + rw_{zz}\right], \tag{4}$$

$$\left(\rho c_p\right)_{hnf} r\left(uT_r + wT_z\right) = k_{hnf}\left[rT_{rr} + T_r + rT_{zz}\right] + \sigma_{hnf} B_0^2 r\left(u^2 + v^2\right) + \frac{16\sigma^* T_\infty^3}{3k^*}\left[rT_{rr} + T_r + rT_{zz}\right] \tag{5}$$

The corresponding boundary constraints are:

$$\left.\begin{array}{lll} u = 0,\ v = \omega r,\ w = 0,\ T = T_w, & \text{at} & z = 0, \\ u = 0,\ v = \Omega r,\ w = 0,\ T = T_\infty, & \text{at} & z = r\tan\alpha, \end{array}\right\} \tag{6}$$

2.1. Lie group transformations

To get requisite similarity variables, a skilled Lie group transformation are adopted [24]. These transformations are as follows:

$$\begin{array}{l} \chi : r^* = r.\exp(\varepsilon\xi_1), z^* = z.\exp(\varepsilon\xi_2), u^* = u.\exp(\varepsilon\xi_3), v^* = v.\exp(\varepsilon\xi_4), \\ w^* = w.\exp(\varepsilon\xi_5), p^* = p.\exp(\varepsilon\xi_6), T^* = T.\exp(\varepsilon\xi_7) \end{array} \tag{7}$$

where the arbitrary real constants $\xi_i (i = 1,.....,7)$ are obtained under invariant conditions, and ε is the Lie group parameter. Introducing Eq. (7) into the governing Eqs. (1) to (5) and equating the exponents, gives:

$$\xi_3 - \xi_1 = \xi_5 - \xi_2, \tag{8}$$

$$2\xi_3 - \xi_1 = 2\xi_4 - \xi_1 = \xi_5 + \xi_3 - \xi_2 = \xi_6 - \xi_1 = \xi_3 - 2\xi_1 = \xi_3 - 2\xi_2 = \xi_3 = \xi_7, \tag{9}$$

$$\xi_3 + \xi_5 - \xi_1 = \xi_5 + \xi_4 - \xi_2 = \xi_4 - 2\xi_2 = \xi_4, \tag{10}$$

$$\xi_3 + \xi_5 - \xi_1 = 2\xi_5 - \xi_2 = \xi_6 - \xi_2 = \xi_5 - 2\xi_1 = \xi_7 - 2\xi_2 = \xi_5 - 2\xi_2, \tag{11}$$

$$\xi_3 + \xi_7 - \xi_1 = \xi_5 + \xi_7 - \xi_2 = \xi_7 - 2\xi_1 = \xi_7 - 2\xi_2 = 2\xi_3 + 2\xi_4 = \xi_1, \tag{12}$$

The solution of Eqs. (8) to (12) yields:

$$\xi_2 = \xi_1, \xi_3 = \xi_4 = \xi_5 = -\xi_1, \xi_6 = -2\xi_1, \xi_7 = 0 \tag{13}$$

Therefore, solving Eqs. (8) to (12) yields the transformation in Eq. (7):

$$\begin{array}{l} \chi : r^* = r.\exp(\varepsilon\xi_1), z^* = z.\exp(\varepsilon\xi_1), u^* = u.\exp(-\varepsilon\xi_1), v^* = v.\exp(-\varepsilon\xi_1), \\ w^* = w.\exp(-\varepsilon\xi_1), p^* = p.\exp(-\varepsilon\xi_6), T^* = T \end{array} \tag{14}$$

Equation (14) yields the following characteristic equations:

$$\frac{dr}{r} = \frac{dz}{z} = \frac{du}{-u} = \frac{dv}{-v} = \frac{dw}{-w} = \frac{dp}{-2p} = \frac{dT}{0} \tag{15}$$

After normalizing and solving Eq. (21), the standard form can be expressed as:

$$r\eta = z,\ ru = \upsilon_f f,\ rv = \upsilon_f g,\ rw = \upsilon_f h,\ r^2 p = \rho_f \upsilon_f^2 P,\ T = T_\infty + \theta(T_w - T_\infty) \tag{16}$$

2.2. Dimensionless Formulas

Equation (16) uses similarity conversions [22, 23]. Non-linear coupled ordinary differential equations can be expressed in dimensionless form as:

$$h' = \eta f', \tag{17}$$

Radial velocity profile:

$$\left.\begin{aligned} & L_f(f,g,h,\theta) + N_f(f,g,h,\theta) = 0 \\ & L_f(f,g,h,\theta) = A_1\left(\eta^2+1\right)f'' + 3A_1\eta f' + 2P + \eta P' - A_3 M f + A_4 Grt\theta, \\ & N_f(f,g,h,\theta) = A_2\left(\eta f - h\right)f' + A_2\left(f^2+g^2\right), \end{aligned}\right\} \tag{18}$$

Azimuthal velocity profile:

$$\left.\begin{aligned} & L_g(f,g,h,\theta) + N_g(f,g,h,\theta) = 0 \\ & L_g(f,g,h,\theta) = A_1\left(\eta^2+1\right)g'' + 3A_1\eta g' + A_2\left(\eta f - h\right)g' - A_3 M g, \\ & N_g(f,g,h,\theta) = A_2\left(\eta f - h\right)g' \end{aligned}\right\} \tag{19}$$

Axial velocity profile:

$$\left.\begin{aligned} & L_h(f,g,h,\theta) + N_h(f,g,h,\theta) = 0 \\ & L_h(f,g,h,\theta) = A_1\left(\eta^2+1\right)h'' + 3A_1\eta h' + A_1 h - P', \\ & N_h(f,g,h,\theta) = A_2\left(\eta f - h\right)h' + \left(A_2 f\right)h, \end{aligned}\right\} \tag{20}$$

Temperature profile:

$$\left.\begin{aligned} & L_\theta(f,g,h,\theta) + N_\theta(f,g,h,\theta) = 0 \\ & L_\theta(f,g,h,\theta) = \left(A_5 + \frac{4}{3}R\right)\left\{\left(1+\eta^2\right)\theta'' - \eta(2n-1)\theta' + n^2\theta\right\} + \Pr Q\theta \\ & N_\theta(f,g,h,\theta) = A_3 \Pr M Ec\left(f^2+g^2\right) - A_6 \Pr\left(\theta'(h-\eta f) + nf\theta\right), \end{aligned}\right\} \tag{21}$$

The respective boundary constraints are:

$$\left.\begin{aligned} & f=0,\ g=Re_w,\ h=0,\ \theta=1, && \text{at} \quad \eta=0 \\ & f=0,\ g=Re_\Omega,\ h=0,\ \theta=0, && \text{at} \quad \eta_0=\tan\alpha \end{aligned}\right\} \tag{22}$$

where,

$$\left.\begin{aligned} & A_1 = \frac{\mu_{hnf}}{\mu_f}, A_2 = \frac{\rho_{hnf}}{\rho_f}, A_3 = \frac{\sigma_{hnf}}{\sigma_f}, A_4 = \frac{(\rho\beta)_{hnf}}{(\rho\beta)_f}, A_5 = \frac{k_{hnf}}{k_f}, A_6 = \frac{(\rho Cp)_{hnf}}{(\rho Cp)_f}, Grt = \frac{g(\beta_T)_f cr^{n+3}}{\upsilon_f^2}, Re_w = \frac{r^2\omega}{\upsilon_f}, \\ & \Pr = \frac{\mu_f (Cp)_f}{k_f}, R = \frac{4\sigma^* T_\infty^3}{k^* k_f}, Ec = \frac{\upsilon_f^2}{(Cp)_f cr^{n+2}}, Q = \frac{Q^* r^2}{\rho_f (Cp)_f \upsilon_f}, Re_\Omega = \frac{r^2\Omega}{\upsilon_f}, M = \frac{\sigma_f B_0^2 r^2}{\rho_f \upsilon_f} \end{aligned}\right\} \tag{23}$$

By removing the pressure term from Eqs. (17), (18) and (20), we obtain:

$$\left.\begin{aligned} & L_f(f,g,h,\theta) = A_1\left(1+\eta^2\right)^2 f''' + \left(1+\eta^2\right)\left\{10A_1\eta + A_2\eta f - A_2 h\right\}f'' - A_3 M f' + A_4 Grt\theta' + 3\left\{2A_1 + 7A_1\eta^2\right\}f' + 3A_1 h \\ & N_f(f,g,h,\theta) = \left(1+\eta^2\right)\left\{A_2\eta f - A_2 h\right\}f'' + 2A_2 g g' + 3\left(A_2 f\right)h + 3\left\{A_2\left(2\eta^2+1\right)f - A_2\eta h\right\}f' \end{aligned}\right\}$$

The pressure component can be obtained from Eq. (20) in the following manner:

$$P = A_1\left(1+\eta^2\right)\eta f' + \eta\left(A_1 + A_2 f\right)h - A_2 h^2 + I \tag{24}$$

Here, I indicates the integrating constant. The heat transmission rates at the disc and cone surfaces are:

$$\begin{aligned} Nu_d &= -\left(\frac{k_{hnf}}{k_f} + R\right)\theta'(0), \\ Nu_c &= -\left(\frac{k_{hnf}}{k_f} + R\right)\theta'(\eta_0) \end{aligned} \tag{25}$$

Table 1. Thermophysical characteristics of hybrid nanofluid.

Viscosity	$\mu_{hnf} = 0.904^2 \exp(14.8(\phi_1 + \phi_2))\mu_f;$
Density	$\rho_{hnf} = (1-\phi_1-\phi_2)\rho_f + \phi_1\rho_1 + \phi_2\rho_2;$
Electrical conductivity	$\frac{\sigma_{hbnf}}{\sigma_{nf}} = \frac{\sigma_2 + 2\sigma_{nf} - 2\phi_2(\sigma_{nf}-\sigma_2)}{\sigma_2 + 2\sigma_{nf} - \phi_2(\sigma_{nf}-\sigma_2)}; \frac{\sigma_{nf}}{\sigma_f} = \frac{\sigma_1 + 2\sigma_f - 2\phi_1(\sigma_f-\sigma_1)}{\sigma_1 + 2\sigma_f + \phi_1(\sigma_f-\sigma_1)};$
Thermal conductivity	$\frac{k_{hnf}}{k_{nf}} = \frac{k_2 + 2k_{nf} - 2(k_{nf}-k_2)\phi_2}{k_2 + 2k_{nf} + (k_{nf}-k_2)\phi_2}; \frac{k_{nf}}{k_f} = \frac{k_1 + 2k_f - 2(k_f-k_1)\phi_1}{k_1 + 2k_f + (k_f-k_2)\phi_1};$
Heat capacitance	$(\rho C_p)_{hnf} = (1-\phi_1-\phi_2)(\rho C_p)_f + \phi_1(\rho C_p)_1 + \phi_2(\rho C_p)_2;$
Thermal expansion coefficient	$(\rho\beta_T)_{hnf} = (1-\phi_1-\phi_2)(\rho\beta_T)_f + \phi_1(\rho\beta_T)_1 + \phi_2(\rho\beta_T)_2;$

Table 2. Properties the base liquid and nanoparticles.

Physical attributes	Water (H_2O)	SWCNT	MWCNT
ρ	997.1	2600	1600
C_p	4179	425	796
k	0.613	6600	3000
σ	5.5×10^{-6}	10^6	10^6

Table 3. Comparison of Nusselt number with published studies.

Model-I	Previous study [25]	Present study
$n = 1$	0.759287	0.7595474533
$n = 2$	0.768	0.7658748775
$n = 3$	0.777035	0.7768466789

3. Results and Discussion

3.1. Conformity of the numerical results with parametric discussion

The integration of single-wall carbon nanotube (SWCNT) and multi-wall carbon nanotube (MWCNT) on the natural convection of water-based hybrid nanofluid past the gap between a rotating cone and a circular disc is presented in this context. The conducting liquid for the interaction of magnetization with the impact of dissipative heat, particularly, viscous and magnetic dissipation enriches the study. Further, gravitation caused by thermal buoyancy and thermal radiation, overshoots the flow profiles significantly. These profiles associated with the thermophysical models consisting of viscosity, density, specific heat, conductivities have the major role on the flow properties and displayed in Table 1. However, the numerical values of the thermal attributes collected from the literatures in standard temperature are deployed in Table 2. The designed governing equations are in dimensional form and therefore needs suitable similarity rules for the transformation in to non-dimensional. Subsequently, the transformed expressions are proposed similarity rule used in the problem converts the standard equations into a non-dimensional form. The angular velocity of the cone is presented as Ω and the circular disc is ω, respectively with corresponding Reynolds number Re_Ω and Re_ω. Depending upon different conditions like the stationary condition as well as rotation of the cone and the circular disc the discussion on the flow phenomena is carried out. Particularly, model I: Stationary disc and rotating cone, model II: stationary cone and rotating disc, model III: co-rotating cone and disc, model IV: counter-rotating cone and disc. Considering all these conditions, the current outcomes are validated with the work of [25] and the numerical results are depicted in Table 3. The tabular results use different Reynolds number against heat transmission rate at the surface of the cone and the circular disc. This validation also provides the convergence criteria of the current methodology adopted for the solution of the system govern by the flow phenomena those are equipped with several factors.

3.2. Streamlines profiles for fixed α

The contributing factors on the proposed designed problem show their significant behaviour for the flow of hybrid nanofluid. Figure 2 characterizes the velocity streamlines in four different models when the rotation angle is $\alpha = \pi/4$. The velocity vectors of a fluid flow field at different point in the form of imaginary lines are termed as velocity streamlines. These are nothing but the tangent to the velocity vectors at each point and also shows the direction in which the fluid element moves. Here, each of the streamlines refers to the velocity magnitude and direction at its location. Moreover, it presents the flow pattern including area of acceleration. Therefore, streamlines never intersect the steady flow field since it represents the path. The analysis of the streamlines is presented for different scenarios. In the case of co-rotating cone and circular disc, particularly $Re_\omega = Re_\Omega = 12$ and the situation of counter rotating cone and disc i.e., $Re_\omega = Re_\Omega = -12$ the flow patterns are away from the surface region. However, farther-apart streamlines represent lower velocities. In both the cases their magnitude seems to be equal due to the same direction of the angular movement. Further, when the cone is in stationary state and the disc is rotating i.e., $Re_\omega = 0, Re_\Omega = 12$ the flow patterns are closer to the surface of the disc and the closer streamlines shows greater velocity in comparison to the streamlines are farther away from it. In case when the rotating cone and stationary disc $(Re_\omega = 12, Re_\Omega = 0)$ condition it little bit away from the surface of the disc. Figure 3 represents the velocity streamlines in the case of $Re_\omega = Re_\Omega = 12$ and varying the rotation angle α representing the angle at which the cone or disc is rotated. At the angle $\alpha = -\pi/3$, the cone or disc rotated in the clockwise direction from the reference position. The velocity streamlines show a combination of radial outward flow and rotational flow around the axis of rotation, with stronger rotational effect dominating as the flow approaches the rotating surface. For $\alpha = -\pi/6$, the cone of disc is rotated in the clock wise of 30° from the reference position. Similar to the previous case, the rotational effect is less pronounced compared to previous angle of rotation. The region of recirculation behind to any of the surface still present but smaller to earlier case. In case the rotational angle $\alpha = \pi/3$, counter-clockwise, the velocity streamlines exhibit a combination of radial outward flow and rotational flow in the opposite direction of the previous two cases. Further, the case is discussed for the rotation angle of $\alpha = \pi/6$ and in this case the region of recirculation is present but the characteristic is different as compared to the opposite rotation direction.

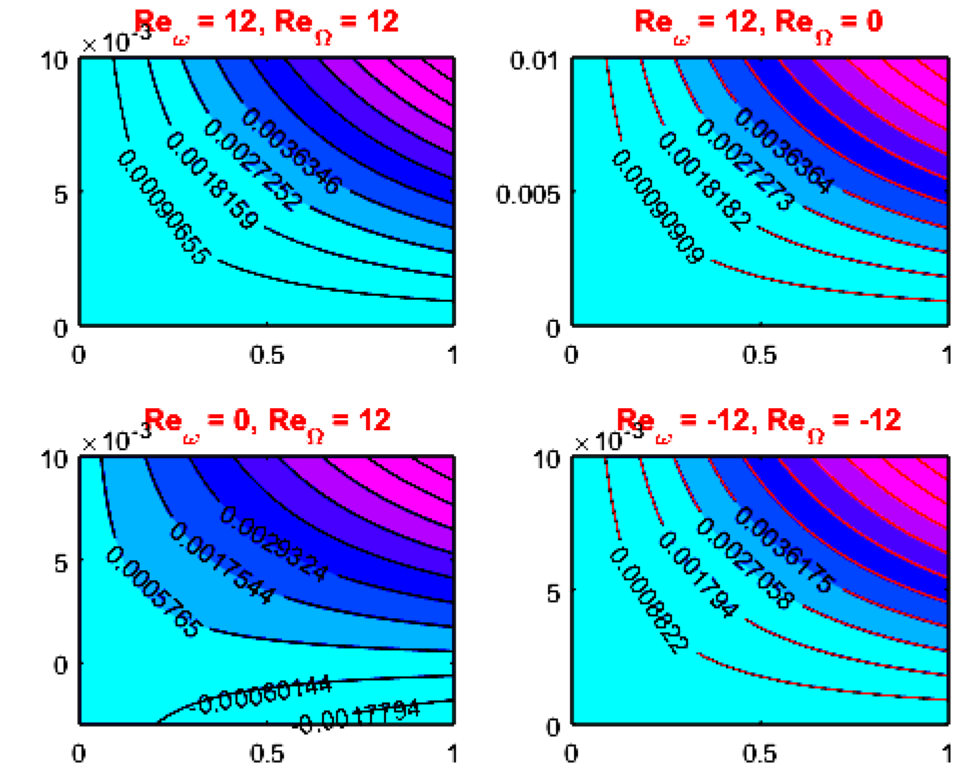

Fig. 2. Velocity streamlines for constant rotation angle.

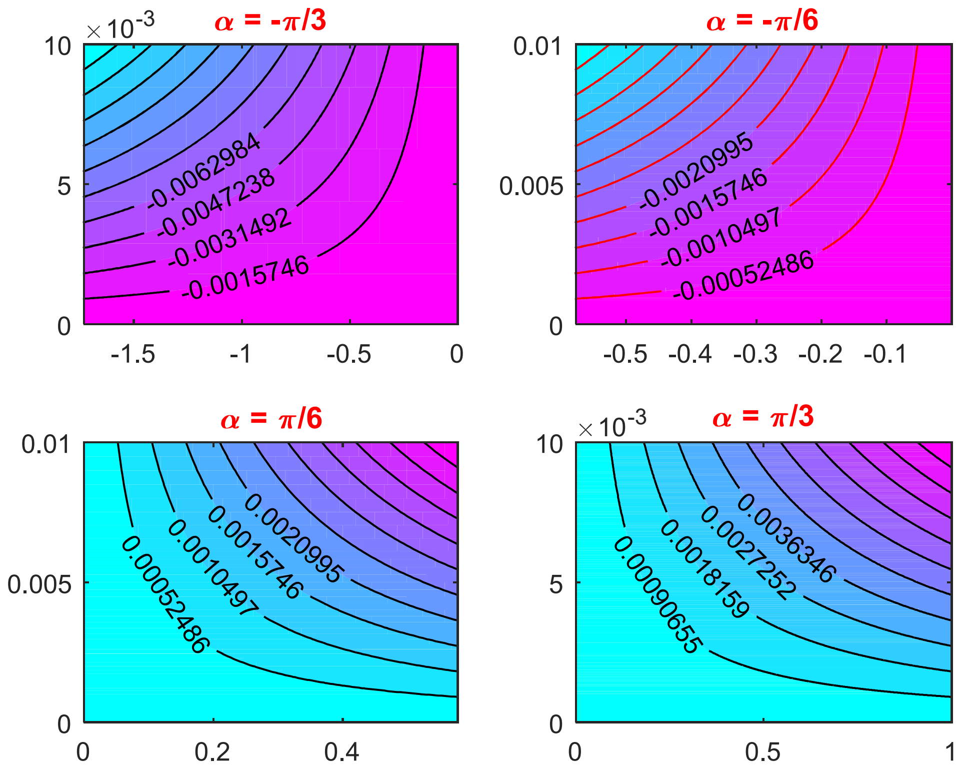

Fig. 3. Velocity streamlines for different rotation angle.

3.3. Behaviour of volume fraction on Nusselt number

The problem of hybrid nanofluid for the combined effect of SWCNT and MWCNT is influenced by the role of the factor volume fraction. The heat transportation properties are boosted due to the interaction of the particle concentration since each of the thermophysical properties are binding with the factor. Figure 4 depicts the characteristic of the volume fraction on the heat transfer rate following two different models such as (i) both the stationary cone and disc (ii) co-rotating cone and disc. The variation of volume fraction of SWCNT nanoparticles are presented in the stationary cone and disc condition for varying heat sink (Q = -0.5) and the absence of heat source (Q = 0). The amount of volume fraction is depicted within the range of 0% to 0.3%. The assigned numeric value $\phi_1 = 0$ represents the case of pure fluid whereas the non-zero volume fraction means the interaction of nanoparticles in the base fluid water (nanofluid). The observation reveals that in both cases, the profiles of heat transmission rate significantly increase near the cone surface but a reverse impact is mounted closer to the disc surface. This fact is rendered due to the density of the concentration for which the agglomerated particles stored energy near the surface and boost up the heat transfer rate. In comparative analysis it is seen that the case of heat sink is more pronounced than the absence of heat source. Again, in the same condition, the impact of volume fraction of MWCNT on the profile of heat transportation is exhibited. As the range of the volume fraction of the nanoparticles is restricted within the range of 0 to 0.3% the profile of heat transfer rate attenuates significantly closer to the surface of the cone but the impact enhances greatly near to the surface of the disc. It is also reflected that absence of heat source is more pronounced than that of the case of heat sink. Further, the variation of the volume fraction of both the CNT nanoparticles considering the co-rotating cone and disc when $Re_\omega = Re_\Omega = 12$. In the proposed case the variation of heat sink and the absence is depicted briefly. In both the cases the rate increases drastically for the increasing volume fraction. This observation reveals due to the rotation of both the cone and the circular disc in counter-clockwise direction. However, the comparative analysis suggests that the heat transmission rate overrides the fact of heat sink i.e., the rate increases in the absence of heat source rather than heat sink.

3.4. Variation of thermal radiation on Nusselt number

Figure 5 portrays the association of thermal radiation on the heat transmission rate considering the cases of nanofluids and hybrid nanofluid. The behaviour is also projected for the varying heat source (Q = 0.5), heat sink (Q = -0.5), and the absence of heat source (Q = 0). Thermal radiation is the electromagnetic wave radiated from the fluid element. This electromagnetic wave is transformed into thermal radiation which radiates temperature from the surface region. Here the range of the thermal radiation is restricted to 0 to 3 for the case of SWCNT water nanofluid considering the variation of heat sink and the absence of heat source. It is noteworthy that for the enhanced thermal radiation the heat transfer rate increases significantly closer to the surface of the cone and this variation is slightly augmented in the absence of heat source. However, the observation is reversed near to the surface of the disc. As the energy radiates from the surface, the surface became cool and the fluid temperature increases. Similar observation revealed for the case of MWCNT nanofluid. The behaviour of thermal radiation is projected for the situation of hybrid nanofluid with varying heat sink and the absence of heat source. The profile increases rapidly for the augmented thermal radiation. The role of heat sink is dominated by the absence of heat source. Further, the behaviour of heat source shows greater augmentation in the heat transfer rate as compared to the sink and the absence of heat source.

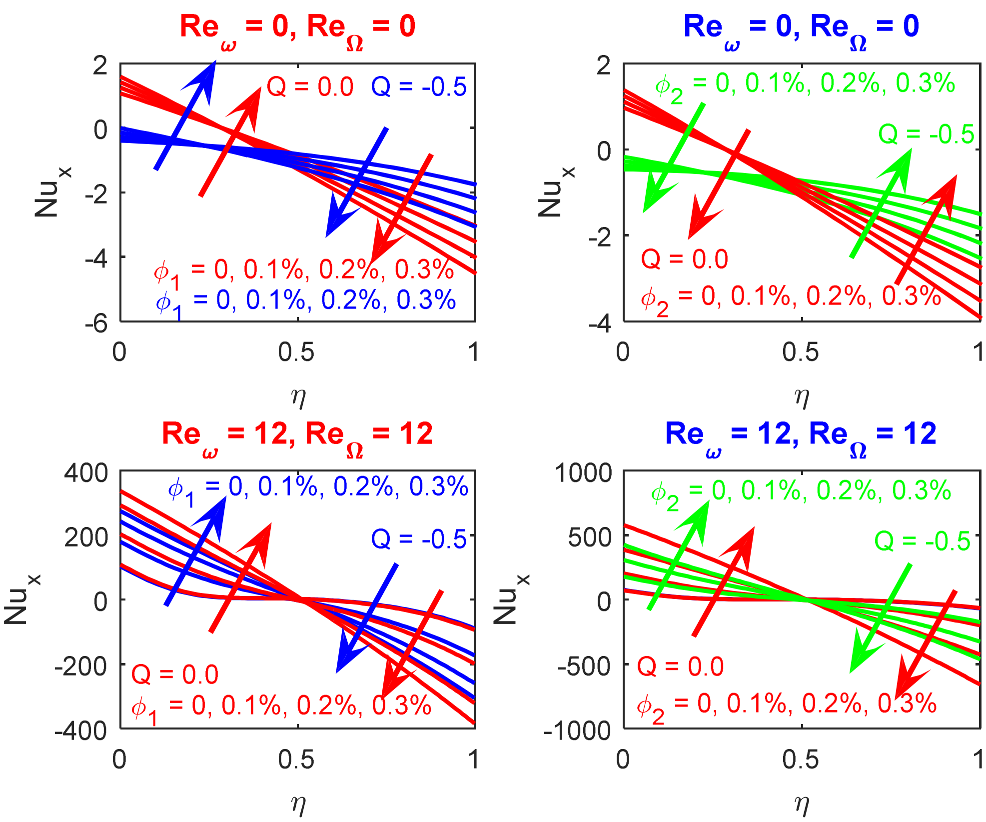

Fig. 4. Nusselt number for the variation of volume fraction.

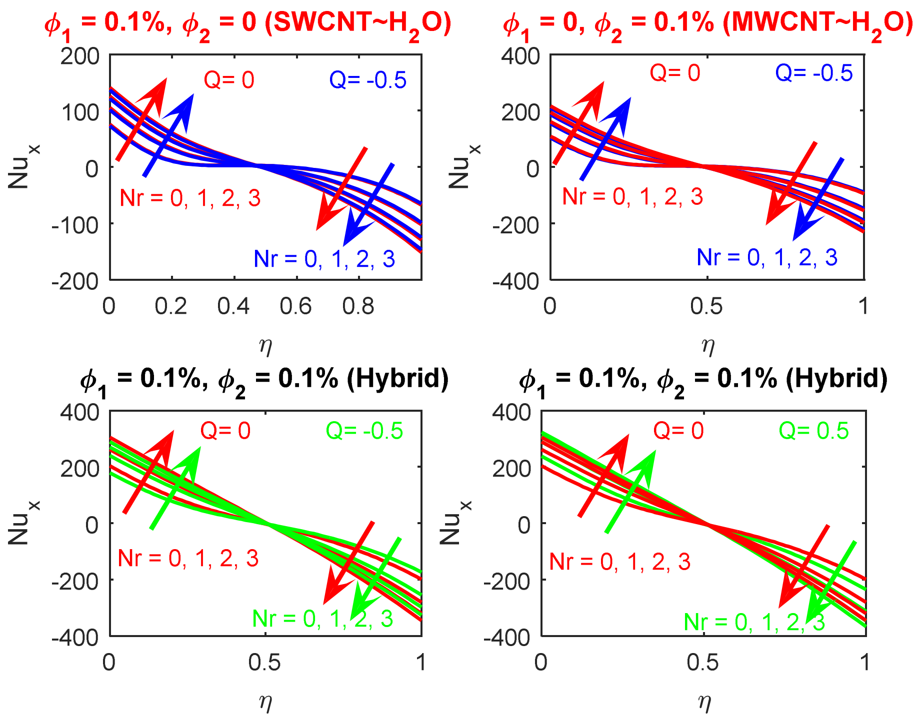

Fig. 5. Nusselt number for the variation of *Nr*.

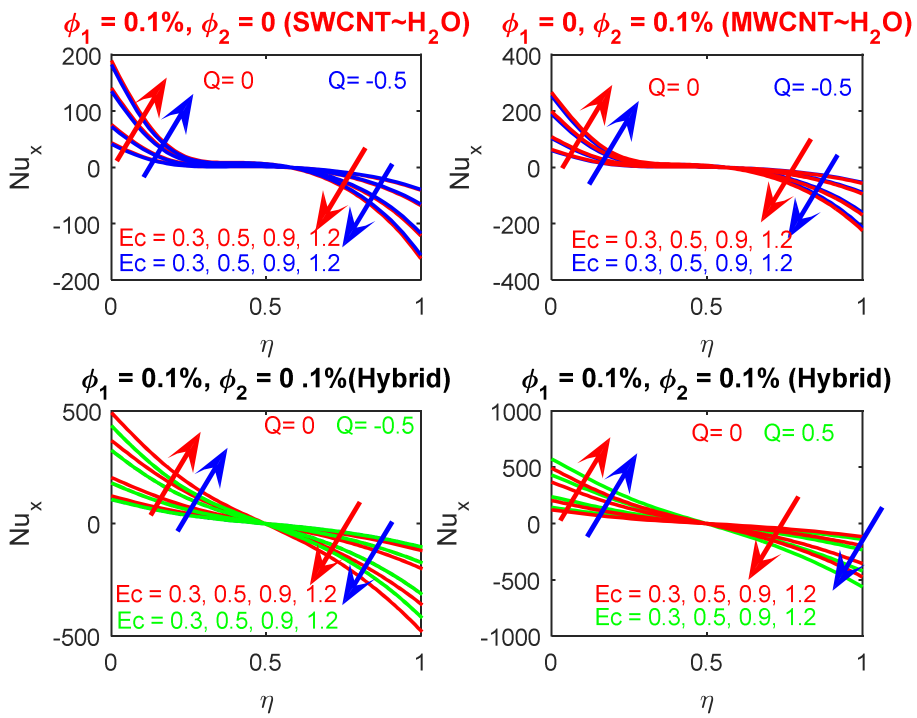

Fig. 6. Nusselt number for the variation of *Ec*.

3.5. Variation of Eckert number on Nusselt number

Figure 6 describes the variation of the Eckert number on the heat transmission rate. The behaviour is depicted for the case of nanofluid as well as the hybrid nanofluid considering the variation of heat source/sink. Eckert number is the quantity which is appeared due to the association of the dissipative heat effect. The dimensionless quantity is defined as the ratio of the kinetic energy with respect to the enthalpy change. The change in enthalpy is due to the convection i.e., the temperature difference between the fluid and the ambient state. The range is restricted within 0.3 to 1.2. The increasing Eckert number suggests the retardation in the enthalpy and this occurs because of the fluid temperature overrides the ambient state temperature. As described for the behaviour of thermal radiation in the previous case, the present case also shows the impact for the variation of heat source/sink for both nanofluid and the hybrid nanofluid it is seen that in case of both the CNT-water nanofluid the heat transfer rate significantly augments near the cone surface. Further, from the point of inflection at the central region the profile retards near the surface of the disc. However, impact is almost similar with different magnitude for the response of heat transfer rate in other cases of hybrid nanofluid. As comparative analysis it is presented that heat source provides maximum strength than that of the heat sink and the absence of heat source.

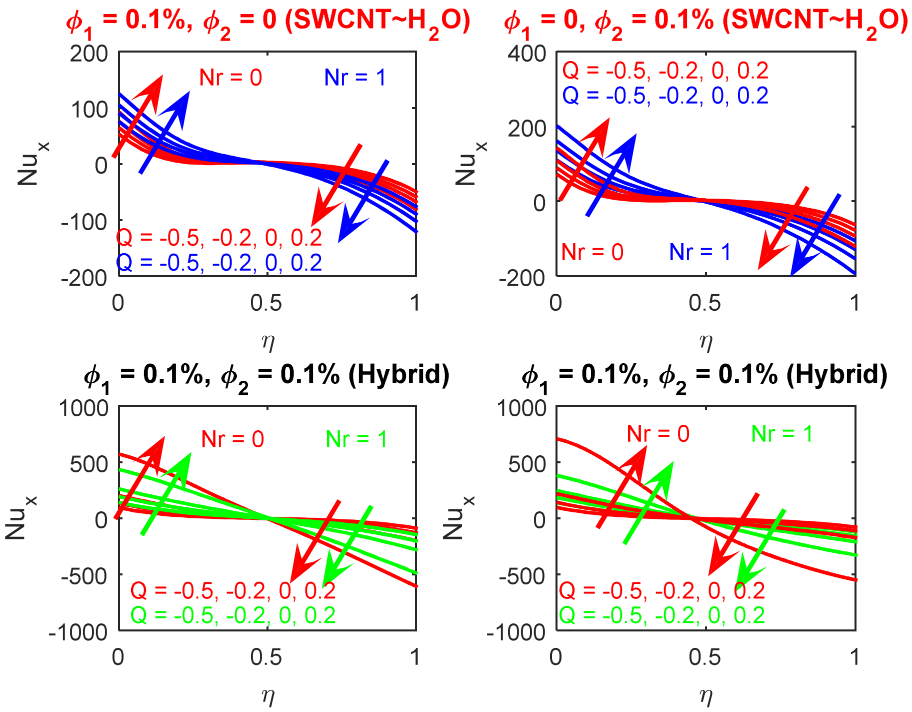

Fig. 7. Nusselt number for the variation of Q and *Nr*.

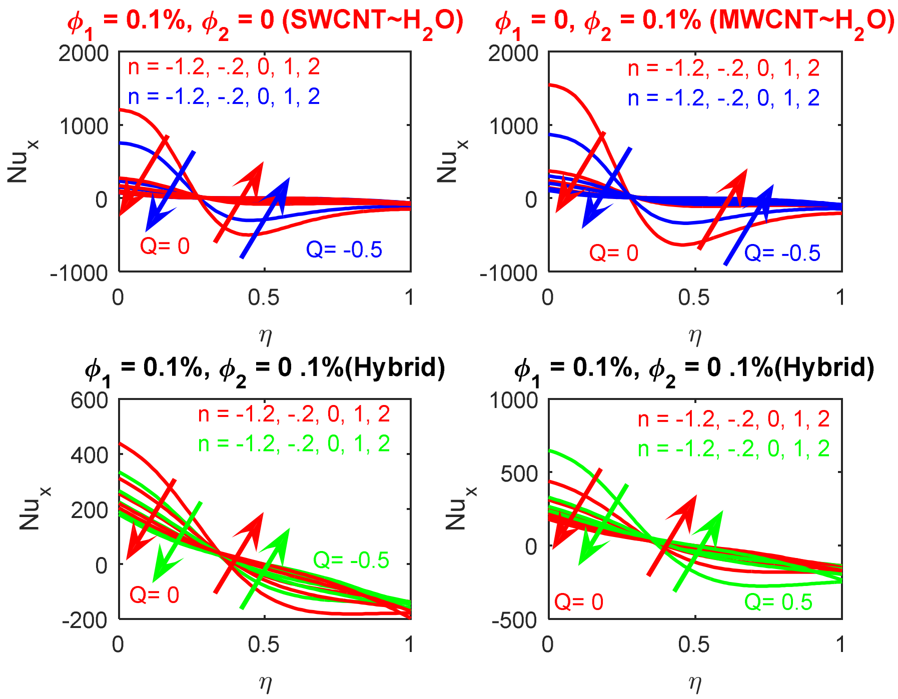

Fig. 8. Nusselt number for the variation of Q and *n*.

3.6. Variation of heat source on Nusselt number

Figure 7 shows the characteristic of heat source/sink on the profiles of the heat transmission rate with varying thermal radiation. The range of the parameter Q is varying within the interval of -0.5 to 0.2 and the observation is projected for the scenarios of nanofluid and hybrid nanofluid. In all these cases the comparative analysis is depicted for the absence of thermal radiation and for the variation it is considered as Nr = 1. The profile shows a dual characteristic from the central region of the proposed domain. With increasing heat source, the profile increases significantly in the case of nanofluid as well as hybrid at the surface of the cone. It is further showing a reverse impact from the central region towards the surface of the disc. However, the comparative analysis shows that the increasing thermal radiation provides greater magnitude in the heat transfer rate. With increasing concentration i.e., for the case of hybrid nanofluid the observation quite similar and the magnitude enhance drastically. It is interesting to reveal the fact that, in case of hybrid nanofluid, the case of heat source is quite destructive and the magnitude of the hike in the profile occurs suddenly. This causes a greater heat transmission rate closer to the cone surface and similarly at the disc surface the greater retardation occurs with same magnitude.

3.7. Variation of power-law index on Nusselt number

The flow phenomena conducted by several thermophysical situations by imposing certain physical condition as described in geometry. However, the surface conditions are also vital in the variation of the profiles. From these conditions, one of the parameters, n, the index parameter has a significant role in varying the surface condition. Figure 8 depicts the variation of index paraeter on the heat transmission rate for different fluids considering the impact of heat source/sink. The range of the parameter is considered as n = -1.2 to 2. Here, it is clear to see, for n = 0, the surface temperature of the cone or the disc is treated as constant whereas for n = 1, the wall temperature behaves linearly. Further, all the other values of the parameter the behavior are nonlinear which affect the profiles greatly. The result reveals that for the case of higher nonlinearity (n = 2) the profile shows ambiguity and hikes drastically near the surface of the cone. As discussed earlier, the profile became smooth in case of hybrid nanofluid and the magnitude increases in case of nanofluid. Therefore, hybrid nanofluid suggests greater stability than the case of nanofluid.

3.8. Variation of magnetic parameter and Reynolds number on azimuthal velocity

Figure 9 demonstrates the influence of magnetization on azimuthal velocity profiles in two scenarios: (i) co-rotation of the cone and disc, and (ii) stationary disc with a rotating cone. The proposed magnetization varies from 0 to 0.8, showcasing that increasing magnetization notably magnifies fluid velocity in both models. In the case of co-rotation (with local Reynolds numbers $\mathrm{Re}_\Omega = \mathrm{Re}_\omega = 12$), velocity profiles exhibit its symmetric nature around the central region, with a notable increase from the surface of the disc towards the middle, followed by deceleration. Conversely, with a stationary disc, velocity upsurges rapidly from the disc surface to the surface of the cone, aligning with boundary conditions. Furthermore, variations in local Reynolds numbers Re_ω and Re_Ω are depicted separately for both circumstances, ranging from 2 to 10. In both cases, enriching the Reynolds number intensifies fluid velocity. Additionally, it is evident that as viscosity obstructs, fluid velocity experiences significant augmentation.

3.9. Variation of magnetic parameter and Reynolds number on axial velocity

Figure 10 displays the axial velocity profiles, presenting the role of varying magnetic parameters and Reynolds numbers on fluid flow. Two distinct patterns are examined: (i) co-rotation of the cone and disc, and (ii) a stationary disc with a rotating cone. Across both cases, the magnetic parameter ranges from 0 to 0.8. The observations in both models, increasing magnetization enhance fluid velocity. Under the co-rotation scenario, where local Reynolds numbers are set at $\mathrm{Re}_\Omega = \mathrm{Re}_\omega = 12$, the velocity profile exhibits symmetric behaviour about the central region. It demonstrates a significant rise from the disc surface towards the midpoint, followed by attenuation with increasing magnitude thereafter. Conversely, with a stationary disc and a rotating cone, the profile experiences rapid augmentation from the disc surface, with enhanced magnitudes evident at the cone surface, aligning with boundary conditions. Additionally, variations in local Reynolds numbers Re_ω and Re_Ω are alternately presented in both scenarios, ranging from 2 to 10. In each case, increasing the Reynolds number correlates with greater fluid velocity, highlighting that as viscous forces diminish, and fluid velocity escalates significantly.

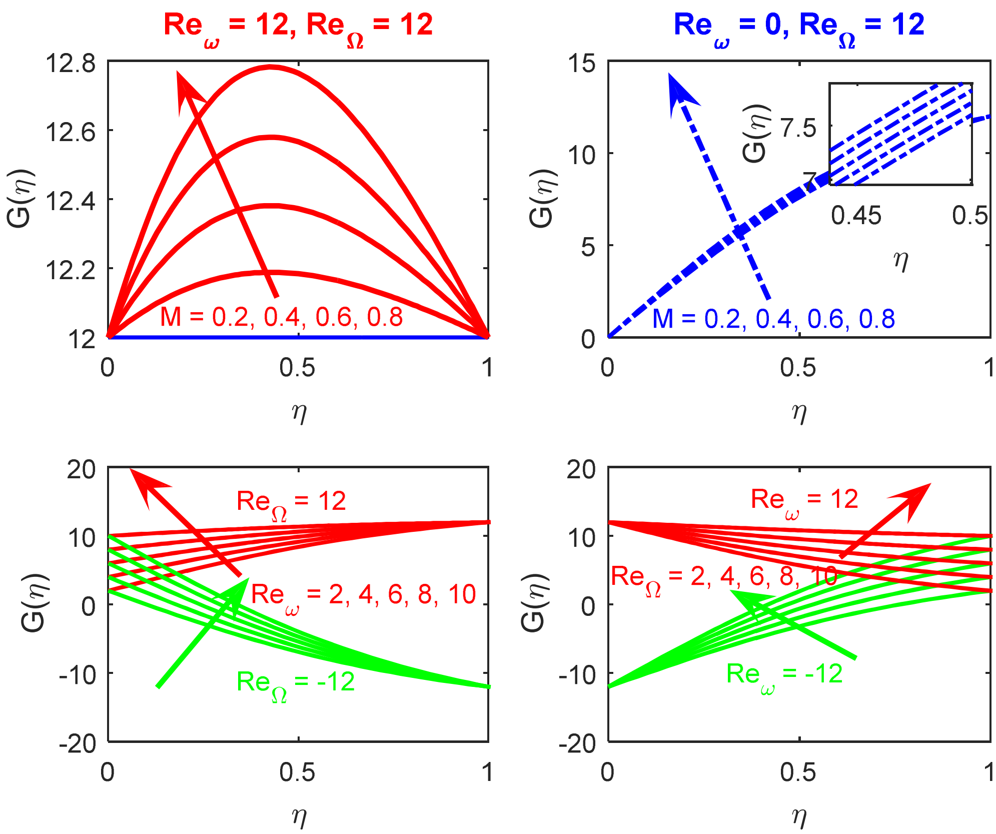

Fig. 9. Azimuthal velocity for the variation of $M, \mathrm{Re}_\Omega, \mathrm{Re}_\omega$.

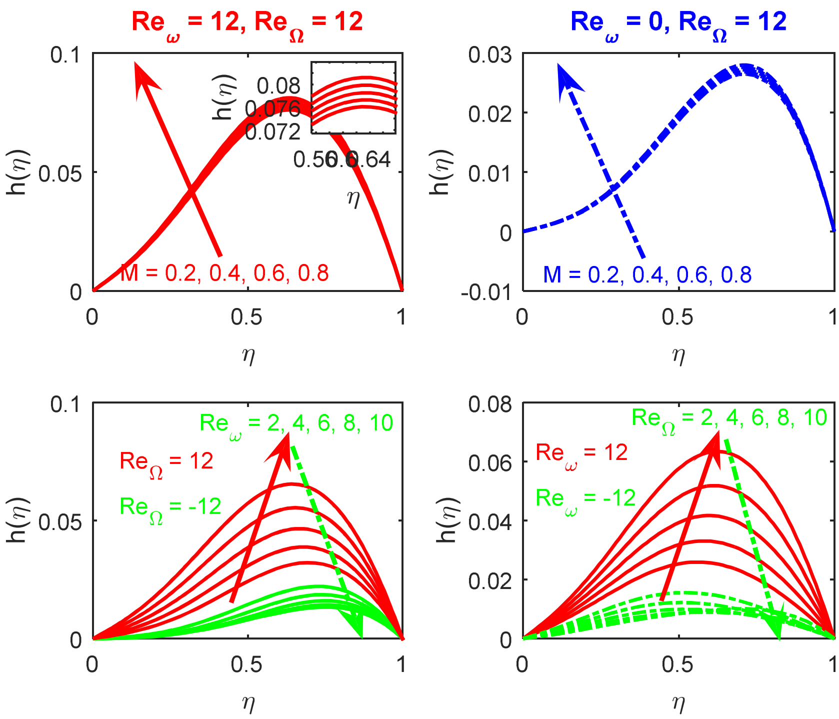

Fig. 10. Axial velocity for the variation of M, Re_Ω, Re_ω .

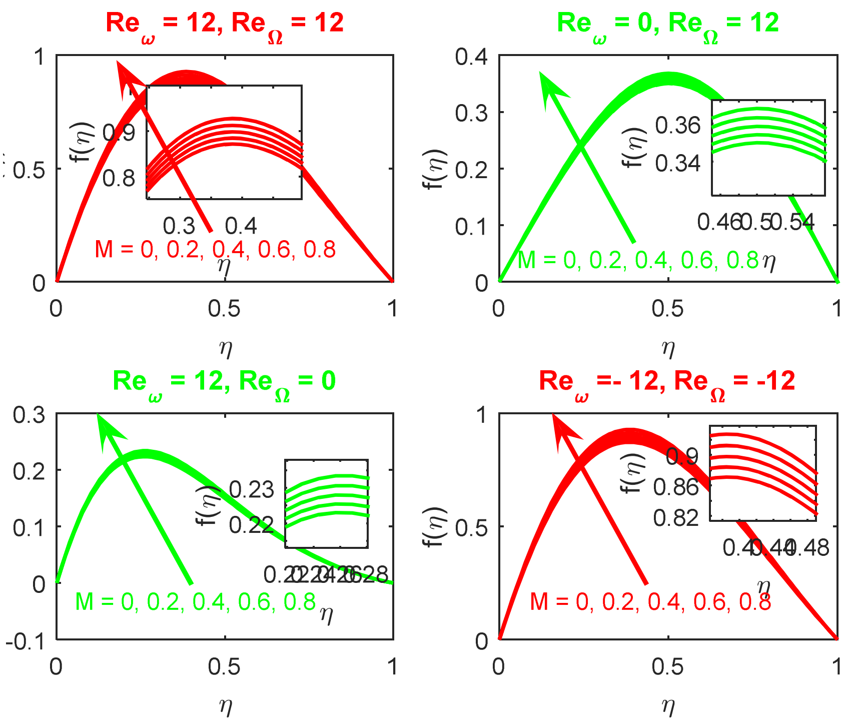

Fig. 11. Radial velocity for the variation of M, Re_Ω, Re_ω .

3.10. Variation of magnetic parameter on radial velocity

The impact of magnetization arises from the applied magnetic field oriented perpendicular to the flow. Figure 11 illustrates the variations in magnetic strength amplify the magnetic field, affecting the radial direction of fluid velocity. The magnetic constraint remains within the range of 0 to 0.8. A parametric value of $M = 0$ indicates the non-existence of a magnetic field, while non-zero values indicate its presence and also provides strength. The insertion of a magnetic field into fluid velocity distribution induces a resistive force known as the "Lorentz force", which opposes the fluid motion. Despite the increasing magnitude in magnetization, there is a notable thickening of the boundary surface, causing velocity profiles to converge closer to the disc surface. The variation of magnetic parameter is detected across four different models, revealing that the absence of a magnetic field results in weaker strength compared to its presence. There is a substantial increase in the profiles exhibit near the disc surface within the domain of $\eta \leq 0.5$, followed by a deceleration. A comparative analysis establishes that in the case of co-rotation or counter rotation of cone and disc, magnitude increases whereas it decreases when the cone remains stationary with a rotating disc.

4. Response Surface Methodology

Response surface methodology (RSM) is a statistical approach employed to model and scrutinize the associations among numerous input variables and one or more response variables. The primary aim of RSM is to enhance the response(s) by identifying the most favorable levels of the input variables. This methodology operates on the premise that the connection between inputs and outputs can be estimated through a polynomial equation. Central Composite Design, as a variant of experimental design under RSM, facilitates the effective investigation of the response surface. It integrates a factorial design with additional center points and axial points, thereby enabling the assessment of curvature and interaction effects as seen in Fig. 12. The design consists of three primary parts:

- **Factorial Design:** In the first stage, a factorial design is used, in which each independent variable is changed at two levels, commonly denoted as -1 and +1. This phase is critical for understanding the main impacts and interactions between variables.
- **Centre Points:** Similar to the factorial design, center points are introduced at the midpoint of each factor's range. These center points are critical for assessing both pure error and curvature in the response surface.
- **Axial Points:** Finally, axial or star points are used to investigate the curvature of the response surface. These points, which are spaced apart along the design space's axes, help to measure the quadratic impacts.

The current simulation takes into account three variables: ϕ_1, ϕ_2, R which are utilized to optimize the local Nusselt number. Table 4 shows the range of effective factors for simulating the heat transportation rate, as well as the distribution of 20 distinct runs with different parameter values. Table 5 shows the R-squared value (100%), which indicates how well the model fits the input data. As a result, the model's accuracy was assessed using ANOVA, with the results presented in Table 6. Standard outcomes are often achieved at a 5% significance level or a 95% confidence level to improve precision. P-values were calculated for the three components based on the ANOVA results, which led to the development of a model that relates to the response with these factors as well as the Nusselt number. The response equation is developed through a rigorous derivation procedure that takes into account a variety of factors and their interactions in order to appropriately reflect the link between input variables as:

$$Nu = -1.19002 - 1.91484A + 1.19006B - 1.58666C + 0.04091A*A - 0.00909B*B - 0.000091C*C + 1.92500A*B + 0.000000A*C + 0.000000B*C \tag{26}$$

After eliminating the insignificant terms:

$$Nu = -1.19002 - 1.91484A + 1.19006B - 1.58666C + 0.04091A*A - 0.00909B*B - 0.000091C*C + 1.92500A*B \tag{27}$$

5. Assessment of Residual, Contour and Surface Plot

Figure 13 depicts a normal plot with data distributions adjusted for fitted values. Along with the data distribution sequence for the Nusselt number response, it shows histograms with the same distribution. In these plots, the residuals almost perfectly fit a straight line, providing strong indication that the model is adequate. Figure 14 shows the contour and surface lines, with the radiation parameter set to a constant central level. The response function increases when the value of A is decreased and B is augmented. Figure 15 shows contour and surface lines, with B at a constant central level. The response function increases as the value of C decreases. Figure 16 depicts contour and surface lines, with A maintained at a constant central level. As C lowers, the response function shows an upward trend, indicating an increase.

Table 4. Experimental design for Nusselt number.

Runs	Coded values			Real values			Response
	A	B	C	ϕ_1	ϕ_2	Rd	Nu_x
1	-1	-1	-1	0.01	0.01	0.1	-1.35574
2	1	-1	-1	0.03	0.01	0.1	-1.39362
3	-1	1	-1	0.01	0.03	0.1	-1.33156
4	1	1	-1	0.03	0.03	0.1	-1.36867
5	-1	-1	1	0.01	0.01	0.3	-1.67308
6	1	-1	1	0.03	0.01	0.3	-1.71096
7	-1	1	1	0.01	0.03	0.3	-1.6489
8	1	1	1	0.03	0.03	0.3	-1.68601
9	-1	0	0	0.01	0.02	0.2	-1.50232
10	1	0	0	0.03	0.02	0.2	-1.53981
11	0	-1	0	0.02	0.01	0.2	-1.53335
12	0	1	0	0.02	0.03	0.2	-1.50879
13	0	0	-1	0.02	0.02	0.1	-1.3624
14	0	0	1	0.02	0.02	0.3	-1.67974
15	0	0	0	0.02	0.02	0.2	-1.52107
16	0	0	0	0.02	0.02	0.2	-1.52107
17	0	0	0	0.02	0.02	0.2	-1.52107
18	0	0	0	0.02	0.02	0.2	-1.52107
19	0	0	0	0.02	0.02	0.2	-1.52107
20	0	0	0	0.02	0.02	0.2	-1.52107

Table 5. Result of R^2 for Nusselt Number.

Source	Sequential p-value	Lack of Fit p-value	Adjusted R^2	Predicted R^2
Linear	< 0.0001	< 0.0001	1.0000	1.0000
2FI	< 0.0001	0.5751	1.0000	1.0000
Quadratic	1.0000	0.3495		
Cubic	1.0000	0.0437		

Table 6. ANOVA test using Quadratic model for Nusselt Number.

Source	Sum of Squares	df	Mean Square	F-value	p-value	
Model	0.2568	6	0.0428	2.002E+10	< 0.0001	significant
ϕ_1	0.0035	1	0.0035	1.644E+09	< 0.0001	
ϕ_2	0.0015	1	0.0015	7.052E+08	< 0.0001	
Rd	0.2518	1	0.2518	1.178E+11	< 0.0001	
$\phi_1 \times \phi_2$	2.928E-07	1	2.928E-07	1.369E+05	< 0.0001	
$\phi_1 \times Rd$	0.0000	1	0.0000	0.0000	1.0000	
$\phi_2 \times Rd$	0.0000	1	0.0000	0.0000	1.0000	
Residual	3.85	10	0.3850			
Lack of Fit	1.640E-11	8	2.050E-12	0.8999	0.5751	
Pure Error	1.139E-11	5	2.278E-12			
Cor Total	0.2568	19				

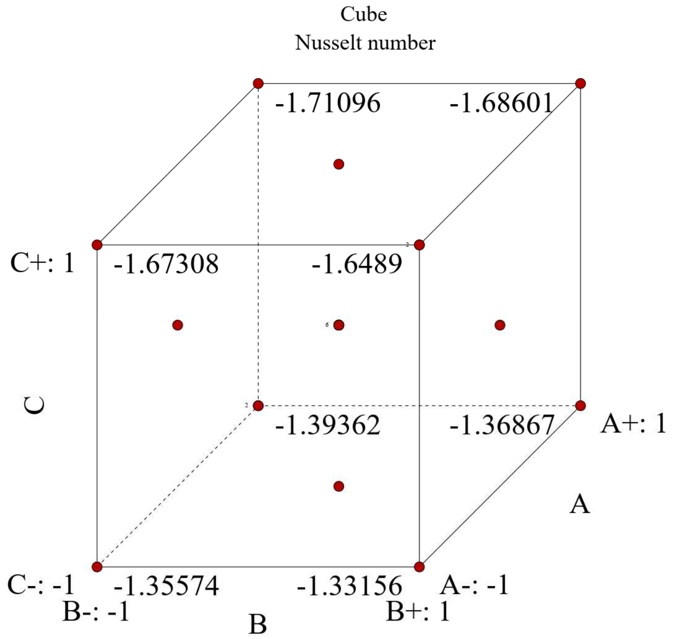

Fig. 12. Central composite design for Nusselt number.

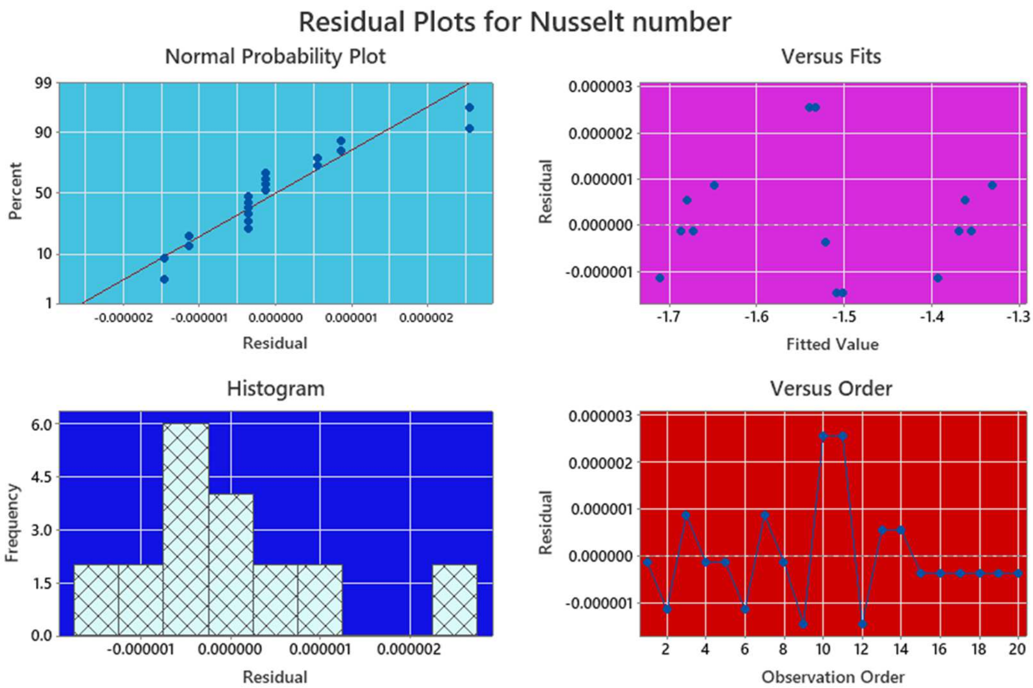

Fig. 13. Residual plot for Nusselt number.

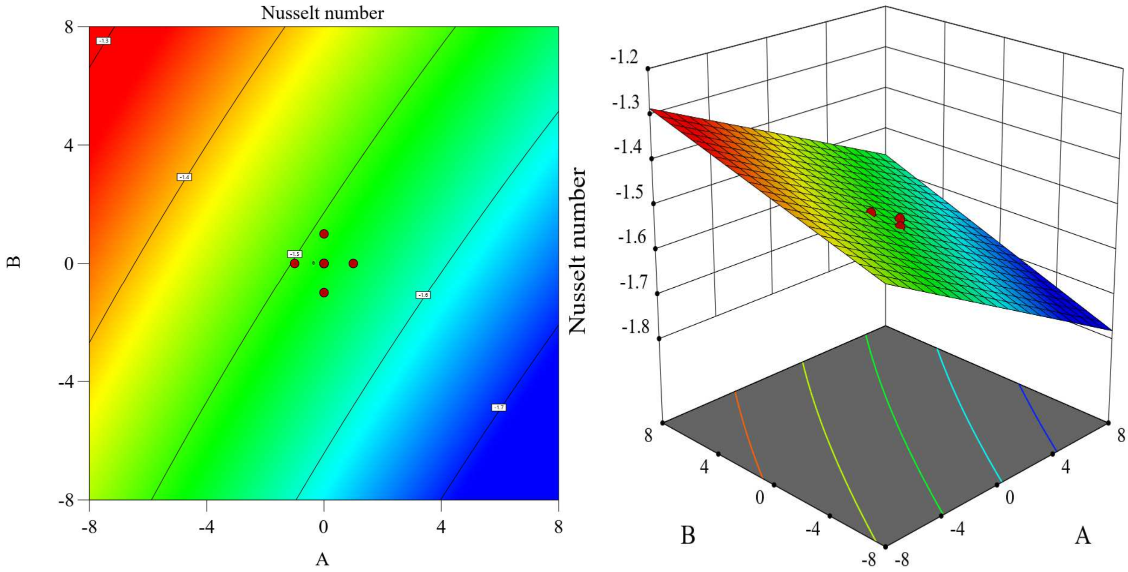

Fig. 14. Contour and surface plot for Nusselt number with C kept as middle value.

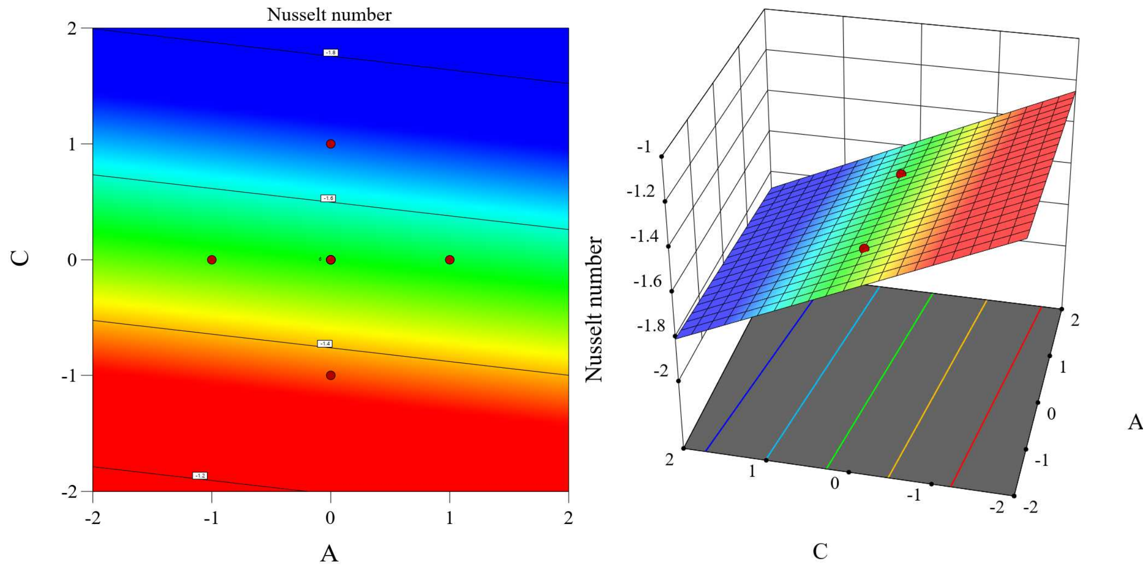

Fig. 15. Contour and surface plot for Nusselt number with B kept as middle value.

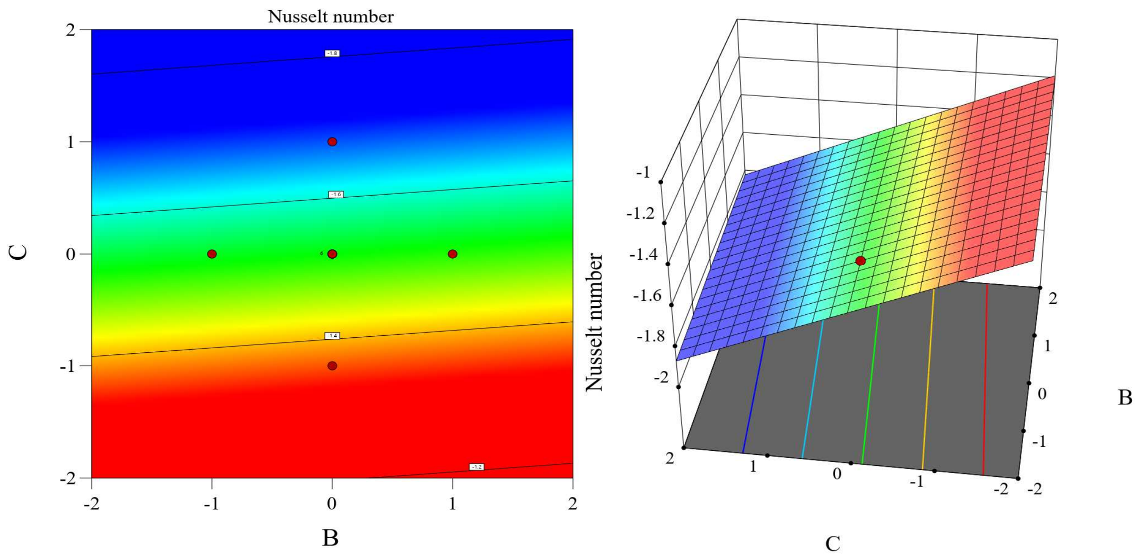

Fig. 16. Contour and surface plot for Nusselt number with A kept as middle value.

6. Conclusion

The electrically conducting CNT-water hybrid nanofluid through the gap between the cone and circular disc for the interaction of dissipative heat and thermal radiation was presented briefly in this work. More importantly, the statistical approach with ANOVA, a hypothetical test was adopted for the optimizing the heat transfer rate analysis for the factors of the volume fraction of both nanoparticles and the thermal radiation was depicted in this study. The structural behaviour of the imported parameters was deployed graphically and elaborated their physical significance briefly. Furthermore, the response surface methodology was used for the effectiveness of the response of heat transfer rate utilizing various factors. Finally, the major outcomes of the results are displayed below:

- The convergence of the proposed methodology is obtained by validating the results of earlier study with the present outcomes in particular case which shows a good correlation numerically.
- The flow pattern presented by the velocity streamlines shows greater velocity for the closed pattern that is viewed with the rotating angel of the cone or the disc in counter-clockwise direction.
- The heat transfer rate of the CNT-water hybrid nanofluid enhances for the increasing volume fraction for the presence of heat sink however the increasing concentration of MWCNT decelerates near the surface of the cone.
- The higher values of the Eckert number and the thermal radiation both upsurges the heat transfer rate near the cone surface and reverse impact is rendered at the surface of the disc.
- The azimuthal fluid velocity hikes for the increasing magnetization in both of the models where co-rotating cone and disc and the rotating dis with stationary cone.
- The axial velocity distribution of the hybrid nanofluid shows significant hike for the enhanced magnetization for the co-rotating or counter rotating of the cone and the disc.

Author Contributions

All authors have equally contributed to the manuscript, R. Baithalu formulated the problem, verified the problem statement, and completed the introduction section, S.R. Mishra computed and simulated the numerical results and finally, S. Panda checked the similarity and grammar and completed the results and discussion section and finally checked the whole text. The manuscript was written through the contribution of all authors. All authors discussed the results, reviewed, and approved the final version of the manuscript.

Acknowledgments

Not applicable.

Conflict of Interest

The authors declared no potential conflicts of interest concerning the research, authorship, and publication of this article.

Funding

The authors received no financial support for the research, authorship, and publication of this article.

Data Availability Statements

The datasets generated and/or analyzed during the current study are available from the corresponding author on reasonable request.

Nomenclature

T	Fluid temperature [K]	c	Stretching rate
T_∞	Ambient temperature	n	Power index
T_w	Wall temperature	(r,ϕ,z)	Cylindrical coordinates
β_T	Volumetric thermal expansion coefficient	B_0	Magnetic strength
ω	Circular disc	Ω	Angular velocity
P	Pressure gradient	Re	Reynolds number
C_p	Specific heat [J/(kg.K)]	ρ	Density
M	Magnetic parameter	Grt	Thermal Grasshof number
R	Thermal radiation [W/m^2]	α	Rotation angle
Q	Heat source [W/m^3]	ϕ	Volume fraction
Ec	Eckert number	Nu	Nusselt number
G	Azimuthal velocity	h	Axial velocity
f	Radial velocity	σ	Electrical conductivity [S/m]
ω	Circular disc	Ω	Angular velocity

References

[1] Raza, Q., Wang, X., Ali, B., Eldin, S. M., Yang, H., Siddique, I., Role of nanolayer on the dynamics of tri-hybrid nanofluid subject to gyrotactic microorganisms and nanoparticles morphology vis two porous disks, *Case Studies in Thermal Engineering*, 51, 2023, 103534.

[2] Panda, S., Pradhan, G., Nayak, D., Pattnaik, P.K., Mishra, S. R., Presentation of entropy due to heat transfer irreversibility of MHD Williamson fluid over an inclined channel, *Modern Physics Letters B*, 38(07), 2023, 2450010.
[3] Mishra, S.R., Pattnaik, P.K., Ontela, S., Panda, S., Characterization of shape factor with multi slip and inclined magnetized radiative Casson hybrid nanofluid transport in an expanding/contracting convective sheet, *Partial Differential Equations in Applied Mathematics*, 8, 2023, 100570.
[4] Rana, P., Gupta, G., FEM solution to quadratic convective and radiative flow of Ag-MgO/H2O hybrid nanofluid over a rotating cone with Hall current: Optimization using Response Surface Methodology, *Mathematics and Computers in Simulation*, 201, 2022, 121-140.
[5] Ramzan, M., Kumam, P., Lone, S.A., Seangwattana, T., Saeed, A., Galal, A.M., A theoretical analysis of the ternary hybrid nanofluid flows over a non-isothermal and non-isosolutal multiple geometries, *Heliyon*, 9(4), 2023, e14875.
[6] Ahmed, S., Chen, Z.M., Xu, H., Ishaq, M., Mixed convection flow in a square lid-driven cavity subject to inclined magnetic field with highly accurate wavelet-homotopy solutions, *Computers & Mathematics with Applications*, 162, 2024, 33-51.
[7] Ahmed, S., Chen, Z.M., Ishaq, M., Multiple solutions in magnetohydrodynamic stagnation flow of hybrid nanofluid past a sheet with mathematical chemical reactions model and stability analysis, *Physics of Fluids*, 35(7), 2023, 072002.
[8] Baithalu, R., Mishra, S.R., Pattnaik, P.K., Panda, S., Optimizing shear and couple stress analysis for the magneto-micropolar dissipative nanofluid flow toward an elongating surface: A comprehensive RSM-ANOVA investigation, *Journal of Thermal Analysis and Calorimetry*, 149, 2024, 1697–1713.
[9] Ahmed, S., Xu, H., Forced convection with unsteady pulsating flow of a hybrid nanofluid in a microchannel in the presence of EDL, magnetic and thermal radiation effects, *International Communications in Heat and Mass Transfer*, 120, 2021, 105042.
[10] Acharya, N., Magnetically driven MWCNT-Fe3O4-water hybrid nanofluidic transport through a micro-wavy channel: A novel MEMS design for drug delivery application, *Materials Today Communications*, 38, 2024, 107844.
[11] Acharya, N., Spectral simulation to investigate the effects of nanoparticle diameter and nanolayer on the ferrofluid flow over a slippery rotating disk in the presence of low oscillating magnetic field, *Heat Transfer*, 50(6), 2021, 5951-5981.
[12] Bartwal, P., Upreti, H., Pandey, A.K., Joshi, N., Joshi, B.P., Application of modified Fourier's law in a fuzzy environment to explore the tangent hyperbolic fluid flow over a non-flat stretched sheet using the LWCM approach, *International Communications in Heat and Mass Transfer*, 153, 2024, 107332.
[13] Upreti, H., Pandey, A.K., Gupta, T., Upadhyay, S., Exploring the nanoparticle's shape effect on boundary layer flow of hybrid nanofluid over a thin needle with quadratic Boussinesq approximation: Legendre wavelet approach, *Journal of Thermal Analysis and Calorimetry*, 148(22), 2023, 12669-12686.
[14] Bartwal, P., Upreti, H., Mishra, S.R., Pandey, A.K., Exploring the features of Von-Karman flow of tangent hyperbolic fluid over a radially stretching disk subject to heating due to porous media and viscous heating, *Modern Physics Letters B*, 2023, DOI: 10.1142/S0217984924501355.
[15] Mishra, S.R., Pattnaik, P.K., Dash, G.C., Effect of heat source and double stratification on MHD free convection in a micropolar fluid, *Alexandria Engineering Journal*, 54, 2015, 681-689.
[16] Francis, P., Sambath, P., Fernandez-Gamiz, U., Noeiaghdam, S., Dinarvand, S., Computational analysis of bio-convective Eyring-Powell nanofluid flow with magneto-hydrodynamic effects over an isothermal cone surface with convective boundary condition, *Heliyon*, 10(3), 2024, e25088.
[17] Ratha, P.K., Mishra. S.R., Tripathy, R.S., Exploration of dissipative heat energy in conjunction with various thermophysical properties of nanofluids: Water and ethylene glycol base fluids, *International Communications in Heat and Mass Transfer*, 138, 2022, 106423.
[18] Li, Y., Mishra, S.R., Pattnaik, P.K., Baag, S., Li, Y., Khan, M.I., Khan, N.B., Alaoui, M.K., Khan, S.U., Numerical treatment of time dependent magnetohydrodynamic nanofluid flow of mass and heat transport subject to chemical reaction and heat source, *Alexandria Engineering Journal*, 61, 2022, 2484-2491.
[19] Thumma, T., Mishra, S.R., Abbas, M.A., Bhatti, M.M., Abdelsalam, S.I., Three-dimensional nanofluid stirring with non-uniform heat source/sink through an elongated sheet, *Applied Mathematics and Computation*, 421, 2022, 126927.
[20] Mahmud, K., Rana, S., Al-Zubaidi, A., Mehmood, R., Saleem, S., Interaction of Lorentz force with cross swimming microbes in couple stress nano fluid past a porous Riga plate, *International Communications in Heat and Mass Transfer*, 138, 2022, 106347.
[21] Shevchuck, I.V., *Convective Heat and Mass Transfer in Rotating Disk Systems*, Springer-Verlag, Berlin, Heidelberg, 2009.
[22] Turkyilmazoglu, M., On the fluid flow and heat transfer between a cone and a disk both stationary or rotating, *Mathematics and Computers in Simulation*, 177, 2020, 329-340.
[23] Wang, F., Rani, S.P., Sarada, K., Gowda, R.P., Zahran, H.Y., Mahmoud, E.E., The effects of nanoparticle aggregation and radiation on the flow of nanofluid between the gap of a disk and cone, *Case Studies in Thermal Engineering*, 33, 2022, 101930.
[24] Olver, P.J., *Applications of Lie groups to differential equations*, Springer Science & Business Media, 1993.
[25] Saini, G., Hanumagowda, B.N., Natural Convective Heat Transfer Analysis of Electrically Conducting Hybrid Nanofluid in a Small Gap Between Rotating Cone and Disc, *BioNanoScience*, 2024, DOI: 10.1007/s12668-024-01308-0.

ORCID iD

Rupa Baithalu https://orcid.org/0000-0003-0672-0140
Subhajit Panda https://orcid.org/0000-0002-4865-0657
S.R. Mishra https://orcid.org/0000-0002-3018-394X

How to cite this article: Baithalu R., Panda S., Mishra S.R. Free Convective Flow of Conducting Hybrid Nanofluid between a Rotating Cone and Circular Disc: Response of Nusselt Number Utilizing Various Factors, *J. Appl. Comput. Mech.*, 11(1), 2025, 82-97. https://doi.org/10.22055/jacm.2024.46643.4563